ACS SENSORS

pubs.acs.org/acssensors

Article

Mechanism and Suppression of Physisorbed-Water-Caused Hysteresis in Graphene FET Sensors

Miroslav Bartošík,* Jindřich Mach, Jakub Piastek, David Nezval, Martin Konečný, Vojtěch Švarc, Klaus Ensslin, and Tomáš Šikola

Cite This: *ACS Sens.* 2020, 5, 2940–2949

Read Online

ACCESS | Metrics & More | Article Recommendations

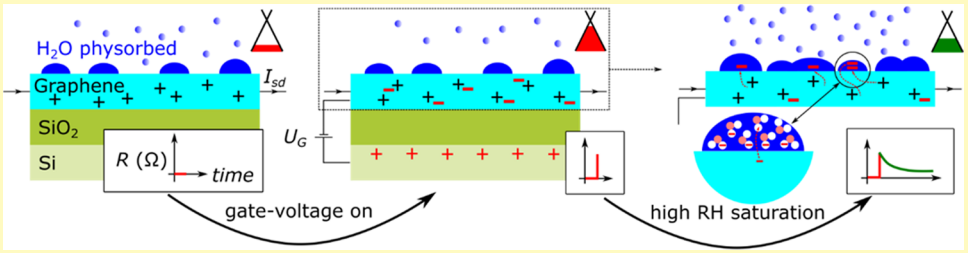

ABSTRACT: Hysteresis is a problem in field-effect transistors (FETs) often caused by defects and charge traps inside a gate isolating (e.g., SiO_2) layer. This work shows that graphene-based FETs also exhibit hysteresis due to water physisorbed on top of graphene determined by the relative humidity level, which naturally happens in biosensors and ambient operating sensors. The hysteresis effect is explained by trapping of electrons by physisorbed water, and it is shown that this hysteresis can be suppressed using short pulses of alternating gate voltages.

KEYWORDS: *graphene, sensor, relative humidity, water, hysteresis, gate voltage, physisorption*

Graphene, a single layer of carbon atoms arranged into a hexagonal structure, is a suitable material for electronic sensors working on the principle of resistivity changes caused by adsorbed molecules acting as acceptors or donors. It has been shown that in vacuum a graphene-based sensor can detect even single gas molecules.[1] This extremely high sensitivity results from the fact that every graphene atom is a surface atom itself and can directly interact with adsorbed particles. Moreover, due to graphene's biocompatibility and ability to be easily functionalized, it can be advantageously used in biosensors operating in air or even in a water solution. Here, in addition to detected molecules, graphene is exposed to water molecules influencing real sensor behavior.[2]

The specific species are usually sensed by graphene sensors (biosensors) having a field-effect transistor (FET) arrangement. The main characteristic for the detection of these species is the dependence of resistivity on back gate voltage (back gate trace) exhibiting a peak corresponding to the charge neutrality point (CNP peak). This point is defined by the Fermi level crossing the Dirac point, where the total charge in graphene should be zero. Ideally, in the case of sensors, the shift of the CNP peak is determined by doping caused by adsorbed molecules being detected. However, the real graphene sensors of a FET's design generally exhibit hysteresis in atmospheric and water solution conditions, consisting in different positions of the CNP peak during upward and downward back gate voltage sweeping. Such a behavior is often attributed to charge trapping and diffusion inside a gate isolating layer (e.g., ion diffusion, negative/positive bias temperature instability).[3−14] This behavior causes ambiguity in the determination of the graphene doping level and the corresponding amount of detected molecules.

In this work, we show that hysteresis in a graphene FET sensor is also caused by water molecules adhered by physisorption. The water origin of this hysteresis is proved by measurements at different relative humidities, under atmospheric conditions and in a vacuum environment caused by water molecules only. Furthermore, it is shown that the hysteresis can be suppressed by the utilization of alternating short gate voltage pulses. Finally, a fundamental mechanism of electron trapping by physisorbed water explaining the hysteresis behavior is proposed.

Received: July 13, 2020
Accepted: September 2, 2020
Published: September 2, 2020

https://dx.doi.org/10.1021/acssensors.0c01441
ACS Sens. 2020, 5, 2940–2949

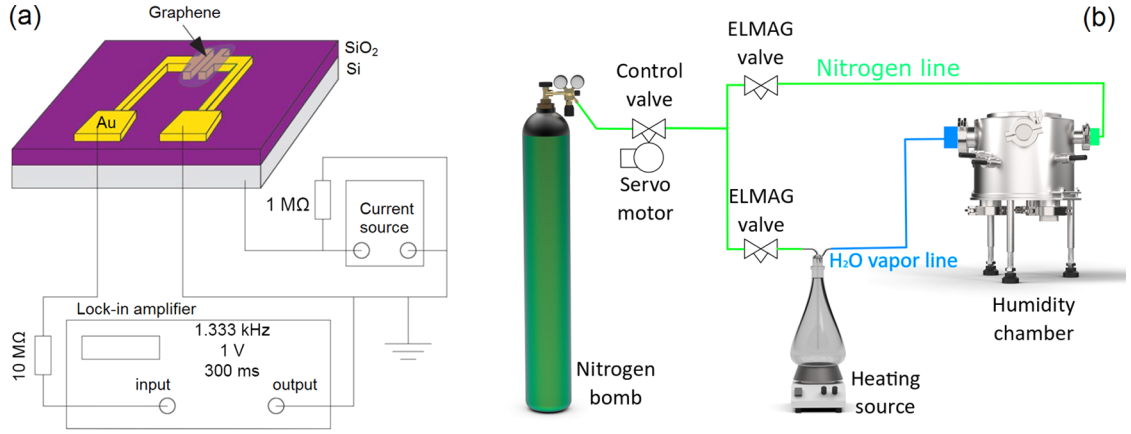

Figure 1. (a) Schematic of the sensor electronic setup for transport measurements. (b) Environmental chamber for controlling the relative humidity.

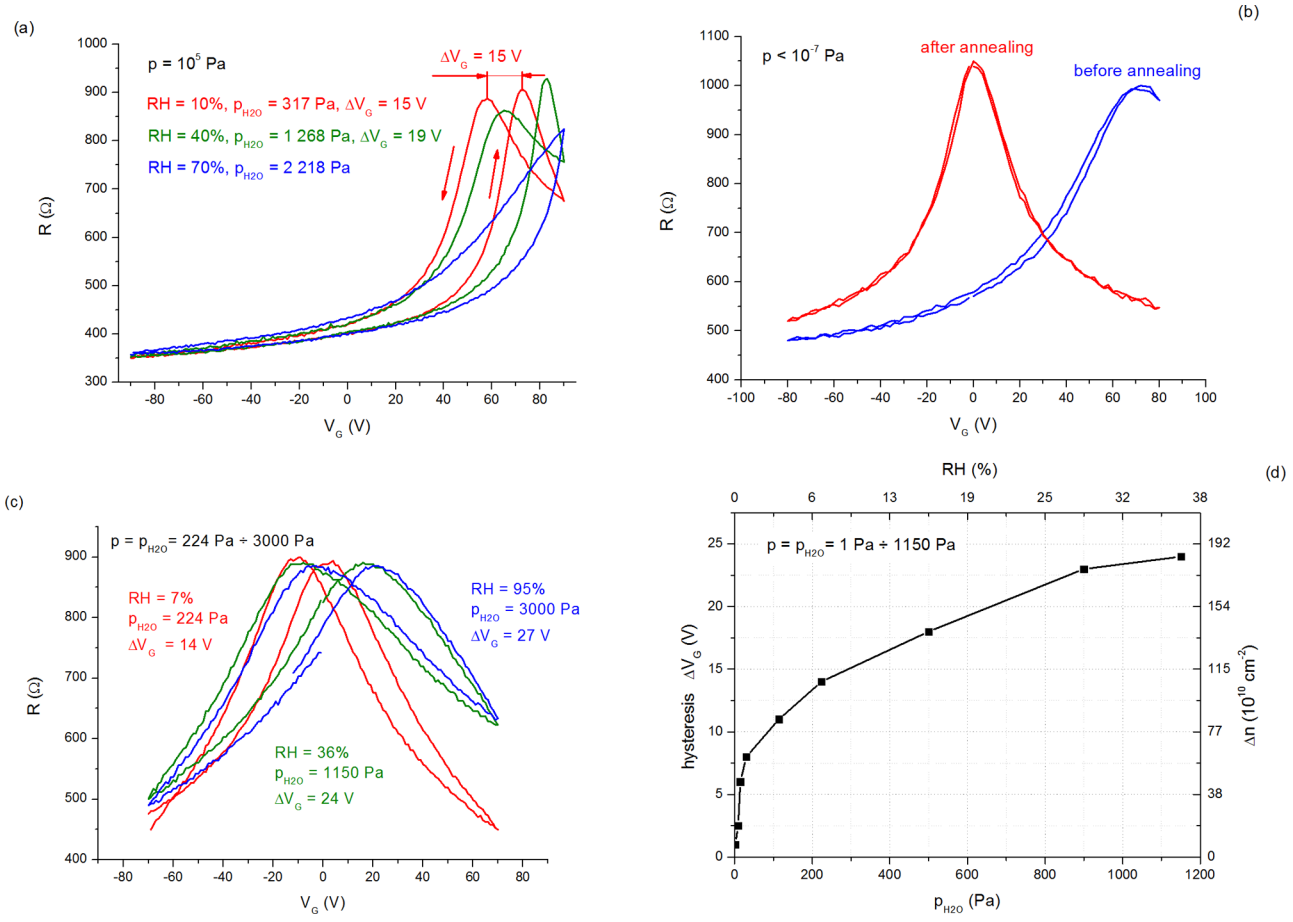

Figure 2. Evolution of hysteresis during the measurement of graphene resistance as a function of back gate voltage: (a) in atmospheric conditions at three different RH values, (b) in UHV before and after annealing (no hysteresis), and (c) in low vacuum at three different water vapor pressures (after introducing water vapors into a UHV chamber). (d) Hysteresis as a function of the pressure of water vapor introduced into a vacuum chamber.

METHODS

A large-area polycrystalline graphene layer was grown by a standard low-pressure chemical vapor deposition (CVD) method.[15] To get a high-quality graphene layer, an ultrasmooth copper foil was used for graphene growth.[16−18] The growth procedure consisted of three technology steps: (1) copper annealing at a hydrogen flow (4 sccm, 10 Pa, 1000 °C, 30 min) to remove air adsorbates, (2) methane introduction (40 sccm, 70 Pa, 1000 °C, 30 min) to grow graphene in a H_2/CH_4 mixture, and (3) bottom-side copper cleaning in oxygen−argon plasma (20% O_2, 80% Ar, 2 min) to remove graphene from this side, while that one from the top side was protected from plasma etching by a spin-coated poly(methyl methacrylate) (PMMA) layer.

The transfer process was performed by a PMMA-assisted wet transfer method. Graphene was transferred on a p-doped silicon substrate (resistivity 1.0×10^{-3}−1.5×10^{-3} Ω·cm) covered by thermal 280 nm SiO_2 and two lithographically prefabricated Au(45 nm)/Ti (3 nm) electrodes. The active part of graphene between these

https://dx.doi.org/10.1021/acssensors.0c01441
ACS Sens. 2020, 5, 2940−2949

electrodes then determines the geometry of the measured graphene channel with length L = 50 μm and width W = 400 μm.

The sample is arranged in the form of a field-effect transistor (FET) with a bottom gate electrode to provide back gate voltage sweeping (Figure 1a). The application of back gate voltage (V_G) controls the charge carrier density according to the formula $n = (\varepsilon_0 e_r/ed)V_G$, where ε_0 is the vacuum permittivity, ε_r is the SiO_2 relative permittivity (3.9), e is the elementary charge, and d is the thickness of the SiO_2 layer. The graphene resistivity is then defined as $\rho = RW/L$, and its dependence on V_G determines the doping type and charge carrier mobility. The resistance (R) of the graphene layer was measured using a lock-in amplifier SR830 (Stanford Research Systems) with a frequency of 1333 Hz, a fixed current of 100 nA, and a back gate voltage in the range of ±90 V.

All transport experiments were measured in situ at the controlled relative humidity (RH) and room temperature of 25 °C (RT). The experiments were carried out either in a home-built stainless steel environmental chamber (Figure 2b) under ambient conditions at atmospheric pressure (10^5 Pa) or in another home-built ultrahigh vacuum (UHV) chamber providing low base pressure (4×10^{-7} Pa) that was increased only by introducing water vapors up to 3000 Pa (corresponding to 95% RH). Nitrogen gas or a water vapor−nitrogen mixture can be flowed through the environmental chamber to reduce or increase the RH in the chamber, respectively.[19] In the UHV chamber, the total pressure is controlled by the evaporation of water from a flask in vacuum.

EXPERIMENTAL RESULTS

Back Gate Trace in Vacuum and Atmosphere at Different RH Values. A typical back gate trace experiment in atmospheric conditions is depicted in Figure 2a. Here, the gate voltage was continuously swept from 0 to 90 V, from 90 to −90 V, and finally from −90 to 0 V. The voltage incremental change during one step was 1 V, and its duration was 0.6 V/s. The measurement was performed at three values of relative humidity: 10, 40, and 70%. Obviously, there are two distinct ways of behavior. First, the curves move toward positive voltages with the relative humidity that corresponds to a stronger p-doping of graphene. Second, the individual curves for each RH do not overlap and exhibit strong hysteresis. For lower RH values of 10 and 40%, the hysteresis can be quantified by a voltage shift (ΔV_G) of the CNP peak, which was 15 and 19 V, respectively. For a higher RH of 70%, the voltage shift parameter cannot be determined due to a strong p-doping, moving the CNP peak out of the measured range. However, even here, a strong hysteresis is present. Generally, the hysteresis causes that the CNP peak is moved to higher gate voltages for increasing gate voltage and to lower gate voltages for decreasing gate voltage during one cycle of back gate trace.

The hysteresis in the measurement leads to ambiguity in the determination of the CNP peak position and consequently influences the calculation of the charge carrier concentration. This ambiguity is possible to quantify. For example, in the case of a back gate trace for 10% RH (red curve in Figure 2a), the right CNP peak occurs at a gate voltage of 74 V and the left peak at 59 V, which corresponds to the mentioned 15 V voltage shift. It results in a charge carrier concentration of 5.7×10^{12} cm^{-2} for the right CNP peak position and 4.54×10^{12} cm^{-2} for the left CNP peak. Therefore, the absolute ambiguity (error) in the determination of the charge carrier concentration is 1.16×10^{12} cm^{-2} and the corresponding relative error in finding this concentration with respect to the mean value is almost 23% (1.16/(5.70 + 4.54)/2). This is quite high value as the changes in the CNP peak position caused by the detected substance in a typical sensor or biosensor are often much smaller.[20−26]

The hysteresis disappeared when the sample was put into the UHV chamber and the pressure was pumped down to 10^{-7} Pa, as can be seen in Figure 2b (blue curve). Furthermore, after annealing at a temperature of 300 °C for 1 h, the CNP peak was shifted from 72 to 1 V (red curve), and the sample again revealed no hysteresis. It leads to the following conclusions. First, the removal of atmospheric molecules in space surrounding the sample eliminated the hysteresis. Second, annealing, which generally removes surface contaminants, adsorbed water molecules, and even water captured under graphene (at the silica−graphene interface),[27] changed the strongly p-doped graphene to intrinsic graphene.

To distinguish between the influences of water and other atmospheric molecules (oxygen, nitrogen, etc.), the annealed sample was exposed in the UHV vacuum chamber to water molecules only, as shown in Figure 2c. Introducing water vapors into the chamber up to the pressure of 3000 Pa (the partial pressure of water molecules is here also an absolute pressure) resulted in the restoration of hysteresis behavior. The voltage shift (ΔV_G) parameters characterizing the hysteresis rate were 14, 24, and 27 for water vapor pressures of 224, 1150, and 3000 Pa, respectively. It corresponds to relative humidity values of 7, 36, and 95%. It means that the hysteresis increased with the amount of water vapor. A more detailed measurement in the relative humidity range from 0 to 36% RH (Figure 2d) showed a gradual exponential saturation of hysteresis development with water vapor pressure ($\approx 23.72 - 20.22 \cdot e^{-0.003 \cdot p}$).

Comparing hysteresis using the back gate voltage shift (ΔV_G) for experiments performed in atmospheric (Figure 2a) and vacuum conditions (Figure 2c), it is obvious that the hysteresis has very similar values for comparable RH values. On the other hand, the average p-doping shift of CNP (calculated from the corresponding left and right peaks in Figure 2c) was close to zero in vacuum (less than 9 V) even after introducing water vapors. From this point of view, the rate of hysteresis in the experiment is related to the level of water vapors present in the sensor's surroundings. However, the overall graphene p-doping relates to ambient conditions since the average p-doping of graphene is recovered after a day of ambient atmosphere exposure. Furthermore (see below discussion), these experimental results will be explained as a consequence of different behaviors of water above and under graphene with RH.

Although the presented experiments performed in vacuum conditions introduced the behavior of the graphene FET sensor exposed to water molecules only, most of the recent biosensors operate in real atmospheric conditions in the presence of all other atmospheric molecules and at the standard pressure. Below, we will focus on sensor behavior in an atmosphere in more detail.

Sensor Response to an Individual Back Gate Voltage Step. Since a typical back gate trace measurement consists of continual gradual changes in back gate voltage, it is fundamental to understand the sensor response on an individual back gate voltage step applied under atmospheric conditions at different RH values. Such a measurement is shown in Figure 3. Here, a single 70 V back gate voltage step was applied at the 100 s time after the beginning of the transport measurement and then the resistance response was observed for the next 160 min. According to practice in sensing experiments,[1,28−32] the relative change of resistance is depicted in Figure 3 instead of the absolute change of resistance. The relative change of

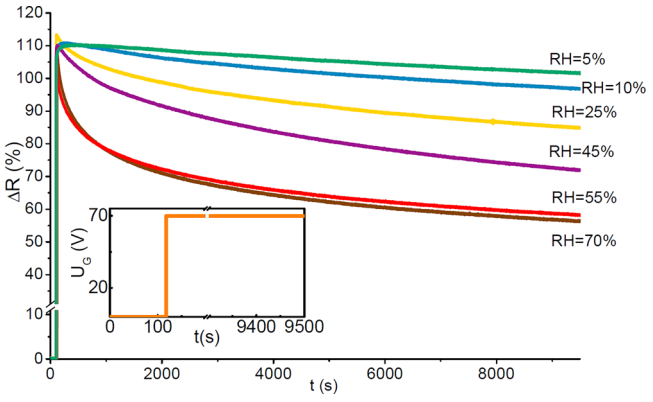

Figure 3. Relative change of sensor resistivity caused by the application of a gate voltage step at the 100 s time from the start of the experiment (see the inset) and its time evolution in the next 160 min under atmospheric conditions for different RH values.

https://dx.doi.org/10.1021/acssensors.0c01441
ACS Sens. 2020, 5, 2940−2949

resistance is defined as $\Delta R = (R(t) - R_0)/R_0$, where $R(t)$ is the resistance measured in time t and R_0 is the initial resistance.

The back gate voltage step results in a big and sudden change in the relative resistance (Figure 3, initial part). This change approaches a value of 110% independent of the relative humidity and is caused by a compensation of the originally p-doped graphene (Figure 2b, blue curve) by the influx of electrons. After the application of gate voltage, a gradual exponential decrease of relative resistance was observed with time (Figure 3, following part). The decay was faster for higher RH values. While for 5% RH (green curve), the resistance remained almost the same (from ΔR = 110% to ΔR = 102%), for 70% RH (brown curve), the relative resistance change decreases to 55% (from ΔR = 110% to ΔR = 55%). Although this exponential decrease occurs within a relatively long time (160 min), it represents one of the main reasons for hysteresis in atmospheric back gate trace measurements (Figure 2a). This is supported by the fact that all of the time during the back gate trace measurements (Figure 2a,c), the resistance also exponentially decreases (Figure 3), while the gate voltage is continually changed.

Sensor Response to a Back Gate Voltage of Different Sizes in UHV and Atmospheric Conditions. The necessity of water vapor presence for the existence of hysteresis in the ambient atmosphere was indirectly confirmed by measurements in UHV (Figure 4), where two gate voltage steps of 28 and 70 V were applied.

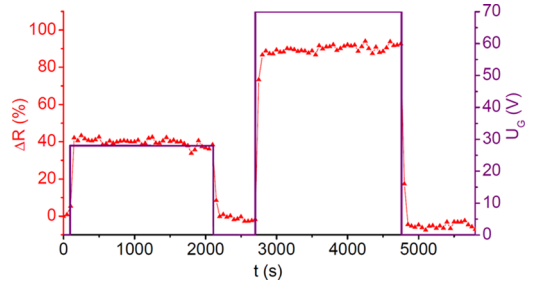

Figure 4. Relative change of sensor resistivity after the application of two gate voltage steps of 28 V (electric field intensity in SiO_2, 1 MV/cm) and 70 V (2.5 MV/cm) and its time evolution in UHV conditions before annealing.

Here, no exponential decrease after switching on the gate voltage was observed, which corresponded to the fact that the back gate trace experiment did not exhibit any hysteresis in UHV (Figure 2b).

The applied back gate voltages of 28 and 70 V resulted in two different electric fields in the SiO_2 layer equal to 1 and 2.5 MV/cm, respectively. Consequently, the lower 28 V gate voltage step caused the lower resistance change ΔR = 40% than the bigger 70 V gate voltage step, which led to ΔR = 90% (Figure 4). The exponential decay is not present in UHV (Figure 4). If these voltages are applied in atmospheric conditions, an exponential decay appears, which is for the lower gate voltage slower in time than for the higher gate voltage (Figure 5a). Here, the relative change of resistance related to the initial maximum R_{max} obtained after the application of the corresponding gate voltage is defined as $\Delta R_{max} = (R(t) - R_{max})/R_{max}$.

The exponential decays depicted in Figures 3 and 5 asymptotically approach a certain saturation value of resistance response. The higher the applied gate voltage and relative humidity, the faster and larger the saturation process. The hypothesis explaining this behavior will be presented in more detail in the Discussion section.

Sensor Response to an Individual Relative Humidity Step. To better understand the resistivity saturation process, the sensor resistance response to a change of relative humidity at the zero gate voltage application was studied. As can be seen in Figure 6, the

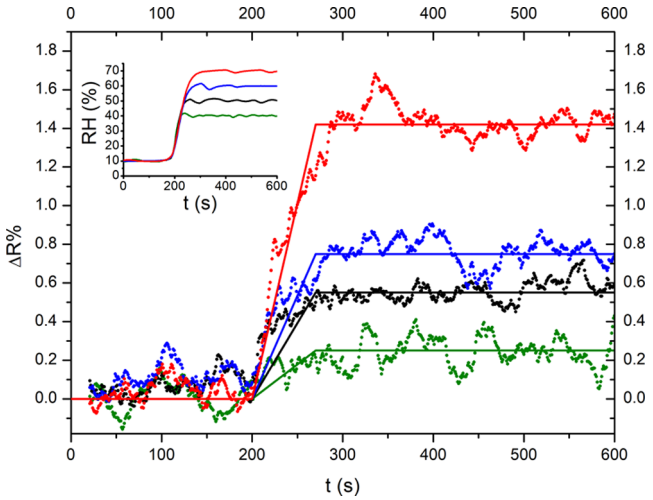

Figure 6. Time development of the relative change of sensor resistivity after the application of four different steplike upturns (inset) of relative humidity at time 200 s: 10 → 40% (green), 10 → 50% (black), 10 → 60% (blue), and 10 → 70% (red).

response is relatively small (<1.6% relative resistance change) and has a relatively long duration (~50 s). Such a small response can be explained by the CNP peak-offset position of the nonannealed graphene utilized in this study, which was higher than 40 V (Figure

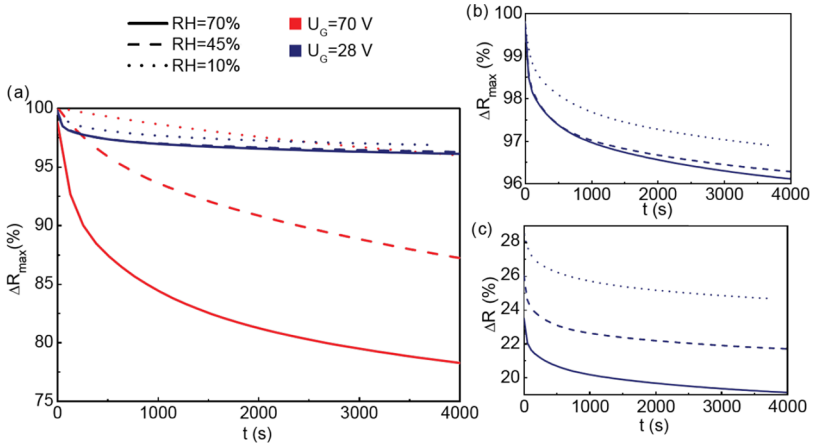

Figure 5. (a) Relative change of sensor resistivity after the application of two gate voltage steps of 28 and 70 V and its time evolution in atmospheric conditions at relative humidities of 10, 45, and 70%. Details of the resistivity relative change for the gate voltage of 28 V related to (b) an initial resistance maximum and (c) initial resistance.

https://dx.doi.org/10.1021/acssensors.0c01441
ACS Sens. 2020, 5, 2940−2949

2a,b, blue curve). Then, at the zero gate voltage application (V_G = 0 V), the resistance can change only slightly since the CNP peak is far away. This problem of small resistance response is usually resolved by setting a proper gate voltage, so that the slope of the resistance course in the back gate voltage trace reaches its highest value—the point of maximum transconductance.[2121] Nevertheless, in our case, such a setting was not possible due to the mentioned process of saturation, while a gate voltage is applied for a longer time. Therefore, in this article, we suggest a different solution presented in the Experimental Solution of the Hysteresis Problem section.

Common Influence of Back Gate Voltage and Relative Humidity. In this section, the response of a graphene FET sensor to steplike relative humidity changes for different gate voltages will be discussed. Such a testing regime is often similar to a working regime of graphene sensors in real operation conditions.[33−36] In Figure 7, the response of the graphene sensor to two relative humidity steps (RH = 10 → 70 → 10 → 70 → 10%) for three different gate voltages of −70, 0, and +70 V is shown. In the case of zero gate voltage, a small resistance response to humidity steps is seen, which is in agreement with our previous measurements (Figure 6, red curve). On the other hand, the reaction to humidity steps is much stronger for the gate voltages of −70 and +70 V (Figure 7, green and red). The charts show the following behavior. First, after the application of these initial gate voltages, the resistance change was swiftly increased and then a long exponential course followed by a saturation occurs. This typical time development was interrupted when a high relative humidity (70%) was applied. In the case of the positive gate voltage application (+70 V, Figure 7, red curve), there is a significant initial positive increase of resistance followed by a lengthy exponential decay, which considerably speeds up during the first humidity step; meanwhile, during the application of the second humidity step, the response is already weak and similar to the zero gate one (black curve). In the case of a negative gate voltage application (−70 V), there is a low initial decrease of resistance followed again by an exponential time development which is increasing in this case. Moreover, the increase is enhanced and accelerated in time of higher humidity steps. The response to the positive gate voltage is in agreement with the previous experiments (Figure 3); however, the response to the negative gate voltage is quite opposite—an initial decrease followed by exponential growth. The lower absolute initial change of resistance and its opposite character can be explained by the asymmetry of the back gate trace curves (Figure 2b, blue curve) since at the application of a negative voltage the resistance decreases and its absolute change is much smaller than that for the positive gate voltage. Both evolutions for positive and negative gates prove the exponential tendency of returning to certain saturated values. Simultaneously, an increase of relative humidity accelerates the process of aiming toward a saturation state. This time evolution process turned on by the gate voltage application is in competition with a small step change of resistivity caused by a change of relative humidity. During the first humidity step (Figure 7), the domination of the returning process is evident; however, in the second step, the real response on humidity prevails. The chart in Figure 7 illustrates how the behavior of sensors can appear complex in a real experiment held in the atmosphere, although it is relatively easy to explain as the interplay of the previously described three partial effects: (1) response to RH, (2) response to gate steps, and (3) motion toward saturation.

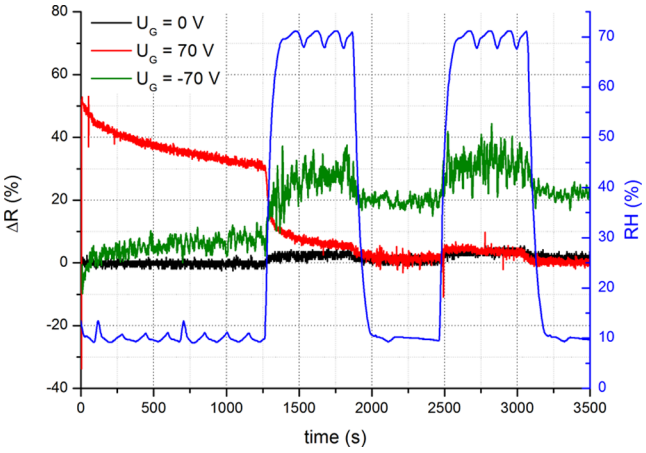

Figure 7. Complex sensor behavior. Relative change of sensor resistivity after the application of two relative humidity steps (10% for 1250 s → 70% for 750 s → 10% for 500 s → 70% for 750 s) at three different gate voltages of 0, +70, and −70 V.

EXPERIMENTAL SOLUTION OF THE HYSTERESIS PROBLEM

The previous experiments have led to the following important results: The response of the sensor to an application of gate voltage in a typical range −90 to +90 V is much stronger than that one to the relative humidity change ranging from 10 to 70%. Moreover, after the gate voltage application, the lengthy process of saturation occurs. However, in common continual back gate trace measurements, an almost immediate change of resistance caused by an applied voltage is required, as the process of the long-lasting saturation (exponential course) brings a side effect of hysteresis into the measurement. With respect to that, it is reasonable to ask how to experimentally resolve the problem of hysteresis and corresponding ambiguity for sensors operating in the atmosphere. This implies a specific question, what is the shortest necessary time to get a full response of a sensor to an application of gate voltage, which would not be significantly distorted by the later saturation process?

To answer this question, an experiment recording the resistance response to gate voltage pulses in small time steps was performed (Figure 8a,c). The resistance response to a gate voltage pulse depicted in Figure 8b is shown in Figure 8d. Here, the resistance was measured in 0.2 s steps after gate voltage switching. The resistance response achieved its full value approximately 2.4 s after the gate voltage application (Figure 8b) and was not affected by the exponential decay within the time interval between 2.4 and 5 s, as depicted in Figure 3.

The problem of the classical back gate trace hysteresis lies in the long time period for which nonzero voltage is applied without interruption and for which the sensor tends to saturate. For example, the positive part of the classical back gate trace from 0 to 90 V and backward takes almost 2 min (180 steps × 0.6 s/step = 1 min 48 s). In comparison with that, the measurement applying the alternating gate voltage eliminates the active time of measurement to 5 s.

To resolve the problem of hysteresis during sensing via back gate voltage tracing, a series of short gate voltage pulses and corresponding resistance responses can be utilized (Figure 8). Such a measurement is free from hysteresis; however, it includes fewer data points than a classical continual back gate trace measurement at the same time due to switching between time-separated discrete back gate voltage pulses. Figure 8a represents the individual measurement cycle composed of 18 gate voltage pulses delayed by one minute.

The experiment comparing a classical continual back gate trace measurement and the modified methodology utilizing alternating gate voltage pulses at three different levels of relative humidity, 40, 70, and 10%, is shown in Figure 9.

Figure 9a,b shows the measurement performed by a standard continual back gate voltage trace. Here, by increasing the back gate voltage, the CNP shifts to the right (more positive gate voltages), and by decreasing the back gate voltage, it shifts to the left. On can see this hysteresis behavior in Figure 9b as an oscillation of the maximum resistance (CNP) point in time depending on the direction of back gate voltage changes.

The results achieved by the application of alternating gate voltage pulses are depicted in Figure 9c,d. Here, the sequence of gate voltages 0 → 10 → 0 → −10 → ... → 80 → 0 → −80 → 0 → 90 → 0 → −90 V was applied (see the inset of Figure 9c). The nonzero value of the back gate voltage was kept for 5 s, while the zero back gate voltage was applied for the rest 55 s to recover the sample from the previously

https://dx.doi.org/10.1021/acssensors.0c01441
ACS Sens. 2020, 5, 2940−2949

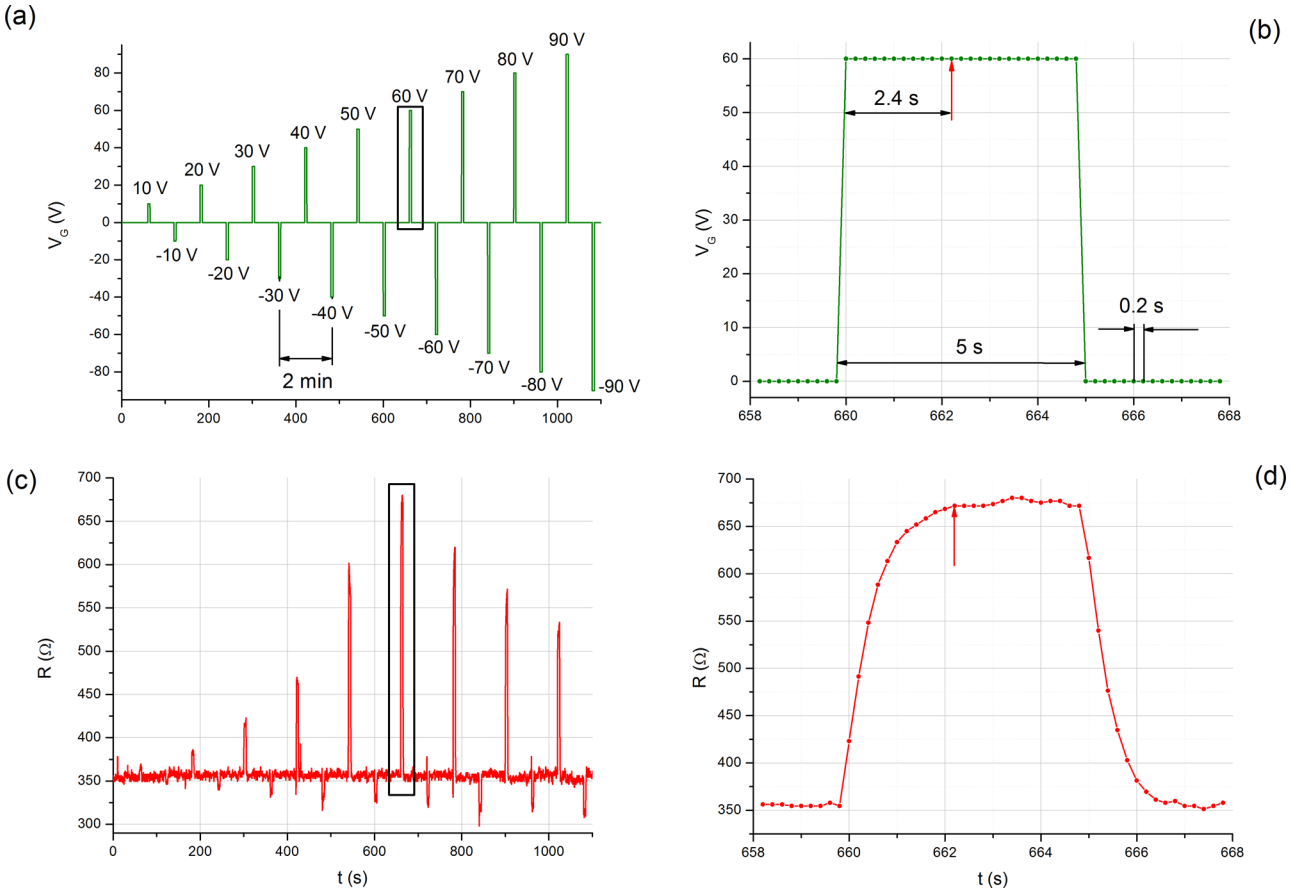

Figure 8. Procedure of a modified back gate trace measurement. (a) Applying a series of alternating gate voltage pulses (each of them lasting for the short time of 5 s) to eliminate the hysteresis effects caused by the exponential saturation time development, (b) details of a positive back gate voltage pulse in one measurement cycle marked in (a) by the black rectangle, (c) resistance response to the series of pulses shown in (a), and (d) details of the resistance response marked in (c) by the black rectangle to the individual gate voltage pulse depicted in (b).

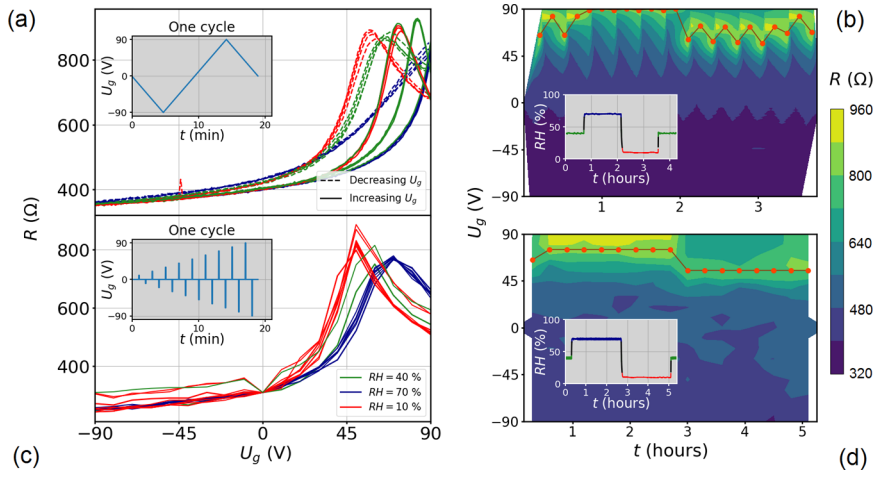

Figure 9. Back gate voltage trace experiment using (a, b) the standard continual procedure (see the inset in (a)) and (c, d) improved method based on alternating back gate voltage pulses (see the inset in (c)) at three relative humidity values of 40, 70, and 10% (see the insets in (b, d)). The positions of maximum resistance (mostly equal to CNP) highlighted by red dots indicate the presence of hysteresis in the case of the standard continual procedure (b) and the absence of hysteresis in the case of the improved method (d).

gate voltage application. The value of resistance was read 2.4 s after the application of the nonzero gate voltage. In measurements done in this way, the hysteresis behavior (the difference between CNP peak positions for increasing and decreasing gate voltages) did not occur (Figure 9c,d), while in the continual back gate trace, the hysteresis was present (Figure 9a,b). At the high relative humidity of 70%, the CNP peak was 80 V (Figure 9c, blue curve), for the low RH = 10%, the CNP peak was 60 V (red curve), and for the middle-level RH = 40%, it was 70 V. Contrary to the standard back gate voltage trace, there is no CNP oscillation and the sensor reacted on the level of RH only. Hence, the utilization of the alternating back gate trace solves the problem of hysteresis by minimization of the time of gate voltage

https://dx.doi.org/10.1021/acssensors.0c01441
ACS Sens. 2020, 5, 2940−2949

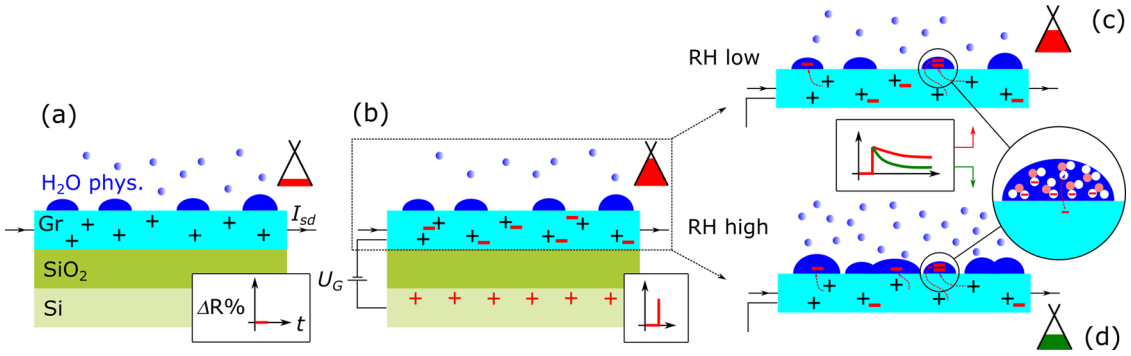

Figure 10. Schematic of the electron trapping mechanism in physisorbed water. (a) Initial state in ambient conditions. (b) Immediate changes after the gate voltage application. (c, d) States after a longer gate voltage application (c) at lower and (d) higher humidity.

application (avoiding the lengthy saturation process) and by application of the zero gate voltage (resuming the original equilibrium in the system).

DISCUSSION

In the previous chapters, the problem of hysteresis accompanying the sensor response in atmospheric conditions, its enhancement with higher humidity, and a solution by the application of short alternating gate voltage pulses instead of the continuous back gate tracing were described. The following questions remain: what is the reason behind the appearance of hysteresis? and what are the fundamental causes of it?

To propose a consistent explanation, two assumptions with respect to water behavior at the graphene−water interface will be made.

First, let us assume that physisorbed water covers the graphene surface at a certain relative humidity. The presence of such a water coverage in the form of droplets was directly proved by Hong et al.[37] using an environmental scanning electron microscope (ESEM). Unlike chemisorbed water (e.g., in the form of OH groups) and water captured under graphene, the amount of water physisorbed on graphene is changing quite flexibly with the relative humidity.

Second, the physisorbed water can bind electrons (due to the relatively high electron affinity reaching a value of 0.8 eV for the water surface[38]). Therefore, water can trap some mobile electrons from graphene and make them immobile. Here, immobility means the removal of electrons from graphene charge carriers. However, the electrons trapped by water can still move by much slower diffusion processes inside the water.

Based on this assumption, the presented experiments can be explained by the mechanism depicted in Figure 10. Initially, the water is physisorbed on the graphene surface proportionally to the relative humidity (Figure 10a). As discussed above, in our experiments, graphene was p-doped (Figure 2). The original graphene p-doping is probably caused by water chemisorbed at the graphene−SiO_2 interface and thus captured under graphene, and only a small fraction of this doping is caused by water physisorbed on top of graphene. At this state, the Fermi level in the graphene cone is below the Dirac point, and hence, the major charge carriers providing the source−drain current (I_{sd}) are holes.

Immediately after the positive gate voltage application, the mobile electrons flow into graphene, shifting the Fermi level up close to the Dirac point and causing a strong resistance increase (Figure 10b).

After that, the electrons from graphene are gradually trapped by water physisorbed on the graphene surface and diffuse deeper into the water droplet (Figure 10c). Due to this continual process, the Fermi level shifts down further from the Dirac point and also the resistance decreases. Since the trapping and diffusion of electrons in water are slow, the process having an exponential time course takes a long time (Figure 3). At higher relative humidity values, the higher amount of physisorbed water can trap more electrons, and consequently, the process is more profound and the resistance decreases more quickly (Figures 10d and 3). Hence, it is worth noting that contrary to the physisorbed water molecules on the graphene surface, the concentration of chemisorbed water molecules captured under graphene is practically independent of RH[27,39] and remains the same (see below).

This phenomenon is similar to the diffusion of charge into a gate-insulating (SiO_2) layer in field-effect transistors (FET)[3−13] observed when this insulating layer contains an increased number of charge traps. These traps are often produced during the fabrication process of the transistor, especially by lithography steps using high-energy particles (e.g., by electron beam lithography) or radiation (e.g., X-ray photons).[40−46] If similar traps were present in our graphene-based FET sensors, then they would exhibit hysteresis and exponential saturation also in UHV conditions, which was not true, as can be seen from Figures 2b and 4. Moreover, the fabrication technology used here was much gentle optical lithography. Hence, based on these facts, the most probable reason for the exponential decrease and saturation of the resistance with time, which is responsible for hysteresis behavior, is the trapping of electrons by physisorbed water.

Generally, the graphene FET can be protected against water molecules by suitable coverage. On the other hand, graphene in biosensors is directly exposed to water solutions, and the presented mechanism of electron trapping by physisorbed water can be crucial.

The relationship between the source−drain current (I_{sd}) used for resistance determination and the applied back gate voltage (U_G) can be described by the following assumption that this current within graphene is dependent on the absolute difference between the Fermi energy (E_F) and the energy of the Dirac point (E_{DP})

$$I_{sd} \sim |E_F - E_{DP}| \quad (1)$$

where the Fermi energy is proportional to the concentration of mobile electrons in graphene (n_{Gr}) as follows[38]

https://dx.doi.org/10.1021/acssensors.0c01441
ACS Sens. 2020, 5, 2940−2949

$$E_F = sgn(n_{Gr})\hbar v_F\sqrt{\pi|n_{Gr}|} \quad (2)$$

Here, $\hbar$ is the reduced Planck constant and v_F is the Fermi velocity of electrons in graphene. The total concentration (n) of electrons, given by the concentration of mobile electrons in graphene (n_{Gr}) and concentration of immobile electrons trapped in physisorbed water on graphene (n_{H_2O}), is proportional to the back gate voltage

$$n = n_{Gr} + n_{H_2O} = \alpha \cdot V_G \quad (3)$$

The current is determined only by electrons remaining in graphene—see eqs 1 and 2. The resultant concentration of these electrons (n_{Gr}) depends on the effectivity of the trapping and diffusion of electrons inside the physisorbed water, which is a lengthy process and takes much time than fast electronic gate switching.

In the proposed model, three different processes can be distinguished according to their speed. First, the fast delivery of electrons into graphene after the application of back gate voltage, taking up to 5 s (Figure 8). Second, the medium-fast process of changing physisorbed water coverage after changing the relative humidity, taking up to 1 min, which was observed by Hong et al.[37] Finally, the slow process of gradual charging of physisorbed water by electrons from graphene and their diffusion into the physisorbed water, taking several minutes and more (Figures 3 and 5).

In the presented explanation, the main responsibility for the hysteresis is carried out by the physisorbed water above graphene whose amount can be easily changed by the relative humidity. On the other hand, part of the physisorbed water is also present under graphene at the silica−graphene interface. However, this water is firmly captured by graphene, which is water-impermeable.[39] The only way through which water can penetrate under graphene is through the edges. This process is however extremely slow and takes days (from 26 h to 70 days) even in the case of a few-micrometer graphene flake on silica completely submerged in water, as proved by Lee et al.[27] However, the onset of hysteresis, when the relative humidity is increased, is almost immediate (Figure 2c). Therefore, we assume that the water under graphene is responsible for overall original p-doping (Figure 2c, blue curve), and after its removal by annealing in vacuum,[27] the sample is almost undoped (Figure 2c, red curve), while the physisorbed water on graphene easily controlled by the RH level is responsible for the occurrence of hysteresis (Figure 2d).

CONCLUSIONS

The ambient transport experiments showed the hysteresis behavior of graphene sensors in a FET configuration increasing with relative humidity and its complete elimination in UHV conditions. The origin of this hysteresis was attributed to the slow trapping of graphene electrons by water physisorbed on graphene, the amount of which is controlled by the relative humidity. It is demonstrated that this problem can be resolved by the application of short alternating gate voltage pulses during back gate trace measurements, allowing the fast electronic processes in graphene and suppressing the slow processes as electron trapping and their diffusion in water. In FET transistors, protection cover layers of graphene can effectively eliminate the problem of hysteresis. However, in the case of FET-based sensors and biosensors, where graphene has to be exposed to ambient and water conditions, the principle and method proposed in this article should be of assistance in understanding and suppression of the hysteresis effect.

AUTHOR INFORMATION

Corresponding Author

Miroslav Bartošík − *Central European Institute of Technology - Brno University of Technology (CEITEC BUT), 612 00 Brno, Czech Republic; Institute of Physical Engineering, Brno University of Technology, 616 69 Brno, Czech Republic; Department of Physics and Materials Engineering, Faculty of Technology, Tomas Bata University in Zlin, 760 01, Czech Republic;* orcid.org/0000-0003-4706-9112; Email: bartosik@fme.vutbr.cz

Authors

Jindřich Mach − *Central European Institute of Technology - Brno University of Technology (CEITEC BUT), 612 00 Brno, Czech Republic; Institute of Physical Engineering, Brno University of Technology, 616 69 Brno, Czech Republic;* orcid.org/0000-0003-1896-0715

Jakub Piastek − *Central European Institute of Technology - Brno University of Technology (CEITEC BUT), 612 00 Brno, Czech Republic; Institute of Physical Engineering, Brno University of Technology, 616 69 Brno, Czech Republic*

David Nezval − *Institute of Physical Engineering, Brno University of Technology, 616 69 Brno, Czech Republic*

Martin Konečný − *Institute of Physical Engineering, Brno University of Technology, 616 69 Brno, Czech Republic*

Vojtěch Švarc − *Central European Institute of Technology - Brno University of Technology (CEITEC BUT), 612 00 Brno, Czech Republic; Institute of Physical Engineering, Brno University of Technology, 616 69 Brno, Czech Republic*

Klaus Ensslin − *Solid State Physics Laboratory, ETH Zürich, CH 8093 Zürich, Switzerland*

Tomáš Šikola − *Central European Institute of Technology - Brno University of Technology (CEITEC BUT), 612 00 Brno, Czech Republic; Institute of Physical Engineering, Brno University of Technology, 616 69 Brno, Czech Republic*

Complete contact information is available at: https://pubs.acs.org/10.1021/acssensors.0c01441

Notes

The authors declare no competing financial interest.

ACKNOWLEDGMENTS

The authors acknowledge the support by the Grant Agency of the Czech Republic (Grant No. 17-21413S), the H2020 Twinning Programme (Project SINNCE, 810626), and MEYS CR (Project No. LQ1601—CEITEC 2020). We also acknowledge the CEITEC Nano Research Infrastructure supported by MEYS CR within the Project LM2015041 for providing us with access to their facilities and Miroslav Kolíbal for reading this manuscript.

REFERENCES

(1) Schedin, F.; Geim, A. K.; Morozov, S. V.; Hill, E. W.; Blake, P.; Katsnelson, M. I.; Novoselov, K. S. Detection of Individual Gas Molecules Adsorbed on Graphene. *Nat. Mater.* **2007**, *6*, 652−655.

(2) Peña-Bahamonde, J.; Nguyen, H. N.; Fanourakis, S. K.; Rodrigues, D. F. Recent Advances in Graphene-Based Biosensor Technology with Applications in Life Sciences. *J. Nanobiotechnol.* **2018**, *16*, No. 95.

(3) Cazalas, E.; Childres, I.; Majcher, A.; Chung, T.-F.; Chen, Y. P.; Jovanovic, I. Hysteretic Response of Chemical Vapor Deposition Graphene Field Effect Transistors on SiC Substrates. *Appl. Phys. Lett.* **2013**, *103*, No. 053123.
(4) Kalon, G.; Shin, Y. J.; Troung, V. G.; Kalitsov, A.; Yang, H. The Role of Charge Traps in Inducing Hysteresis: Capacitance−Voltage Measurements on Top Gated Bilayer Graphene. *Appl. Phys. Lett.* **2011**, *99*, No. 083109.
(5) Liao, Z.-M.; Yan, B.-H.; Zhou, Y.-B.; Yu, D.-P. Hysteresis Reversion in Graphene Field-Effect Transistors. *J. Chem. Phys.* **2010**, *133*, No. 044703.
(6) Joshi, P.; Romero, H. E.; Neal, A. T.; Toutam, V. K.; Tadigadapa, S. A. Intrinsic Doping and Gate Hysteresis in Graphene Field Effect Devices Fabricated On. *J. Phys.: Condens. Matter* **2010**, *22*, No. 335214.
(7) Kuhn, M.; Silversmith, D. J. Ionic Contamination and Transport of Mobile Ions in MOS Structures. *J. Electrochem. Soc.* **1971**, *118*, 966−970.
(8) Lafkioti, M.; Krauss, B.; Lohmann, T.; Zschieschang, U.; Klauk, H.; Klitzing, K.; Smet, J. H. Graphene on a Hydrophobic Substrate: Doping Reduction and Hysteresis Suppression under Ambient Conditions. *Nano Lett.* **2010**, *10*, 1149−1153.
(9) Levesque, P. L.; Sabri, S. S.; Aguirre, C. M.; Guillemette, J.; Siaj, M.; Desjardins, P.; Szkopek, T.; Martel, R. Probing Charge Transfer at Surface Using Graphene Transistors. *Nano Lett.* **2011**, *11*, 132−137.
(10) Shi, Y.; Fang, W.; Zhang, K.; Zhang, W.; Li, L. Photoelectrical Response in Single-Layer Graphene Transistors. *Small* **2009**, *5*, 2005−2011.
(11) Wang, H.; Wu, Y.; Cong, C.; Shang, J.; Yu, T. Hysteresis of Electronic Transport in Graphene Transistors. *ACS Nano* **2010**, *4*, 7221−7228.
(12) Xu, H.; Chen, Y.; Zhang, J.; Zhang, H. Investigating the Mechanism of Hysteresis Effect in Graphene Electrical Field Device Fabricated on SiO_2 Substrates Using Raman Spectroscopy. *Small* **2012**, *8*, 2833−2840.
(13) Krishnan, A. T.; et al. Negative Bias Temperature Instability Mechanism: The Role of Molecular Hydrogen. *Appl. Phys. Lett.* **2006**, *88*, No. 153518.
(14) Konečný, M.; Bartošík, M.; Mach, J.; Švarc, V.; Nezval, D.; Piastek, J.; Procházka, P.; Cahlík, A.; Šikola, T. Kelvin Probe Force Microscopy and Calculation of Charge Transport in a Graphene/Silicon Dioxide System at Different Relative Humidity. *ACS Appl. Mater. Interfaces* **2018**, *10*, 11987−11994.
(15) Li, X.; Cai, W.; An, J.; Kim, S.; Nah, J.; Yang, D.; Piner, R.; Velamakanni, A.; Jung, I.; Tutuc, E.; et al. Large Area Synthesis of High Quality and Uniform Graphene Films on Copper Foils. *Science* **2009**, *324*, 1312−1314.
(16) Procházka, P.; Mach, J.; Bischoff, D.; Lišková, Z.; Dvořák, P.; Vaňatka, M.; Simonet, P.; Varlet, A.; Hemzal, D.; Petrenec, M.; et al. Ultrasmooth Metallic Foils for Growth of High Quality Graphene by Chemical Vapor Deposition. *Nanotechnology* **2014**, *25*, No. 185601.
(17) Mach, J.; Procházka, P.; Bartošík, M.; Nezval, D.; Piastek, J.; Hulva, J.; Švarc, V.; Konečný, M.; Kormoš, L.; Šikola, T. Electronic Transport Properties of Graphene Doped by Gallium. *Nanotechnology* **2017**, *28*, No. 415203.
(18) Mach, J.; Šamořil, T.; Kolíbal, M.; Zlámal, J.; Voborny, S.; Bartošík, M.; Šikola, T. Optimization of Ion-Atomic Beam Source for Deposition of GaN Ultrathin Films. *Rev. Sci. Instrum.* **2014**, *85*, No. 083302.
(19) Bartošík, M.; Kormoš, L.; Flajšman, L.; Kalousek, R.; Mach, J.; Lišková, Z.; Nezval, D.; Švarc, V.; Šamořil, T.; Šikola, T. Nanometer-Sized Water Bridge and Pull-off Force in AFM at Different Relative Humidities: Reproducibility Measurement and Model Based on Surface Tension Change. *J. Phys. Chem. B* **2017**, *121*, 610−619.
(20) Ohno, Y.; Maehashi, K.; Yamashiro, Y.; Matsumoto, K. Electrolyte-Gated Graphene Field-Effect Transistors for Detecting PH and Protein Adsorption. *Nano Lett.* **2009**, *9*, 3318−3322.
(21) Fu, W.; Feng, L.; Panaitov, G.; Kireev, D.; Mayer, D.; Offenhäusser, A.; Krause, H. Biosensing near the Neutrality Point of Graphene. *Sci. Adv.* **2017**, *3*, No. e1701247.
(22) Vieira, N. C. S.; Borme, J.; Machado, G.; Cerqueira, F.; Freitas, P. P.; Zucolotto, V.; Peres, N. M. R.; Alpuim, P. Graphene Field-Effect Transistor Array with Integrated Electrolytic Gates Scaled To. *J. Phys.: Condens. Matter* **2016**, *28*, No. 085302.
(23) Fu, W.; Jiang, L.; van Geest, E. P.; Lima, L. M. C.; Schneider, G. F. Sensing at the Surface of Graphene Field-Effect Transistors. *Adv. Mater.* **2017**, *29*, No. 1603610.
(24) Cheng, Z.; Li, Q.; Li, Z.; Zhou, Q.; Fang, Y. Suspended Graphene Sensors with Improved Signal and Reduced Noise. *Nano Lett.* **2010**, *10*, 1864−1868.
(25) Ang, P. K.; Chen, W.; Wee, A. T. S.; Loh, K. P. Solution-Gated Epitaxial Graphene as PH Sensor. *J. Am. Chem. Soc.* **2008**, *130*, 14392−14393.
(26) Ohno, Y.; Maehashi, K.; Matsumoto, K. Label-Free Biosensors Based on Aptamer-Modified Graphene Field-Effect. *J. Am. Chem. Soc.* **2010**, *132*, 18012−18013.
(27) Lee, D.; Ahn, G.; Ryu, S. Two-Dimensional Water Diffusion at a Graphene−Silica Interface. *J. Am. Chem. Soc.* **2014**, *136*, 6634−6642.
(28) Hwang, S.; Lim, J.; Goo, H.; Kyun, W.; Kim, D.; Sang, I.; Hun, J.; Lee, S.; Ha, D.; Chan, S. Chemical Vapor Sensing Properties of Graphene Based on Geometrical Evaluation. *Curr. Appl. Phys.* **2012**, *12*, 1017−1022.
(29) Popov, V. I.; Nikolaev, D. V.; Timofeev, V. B.; Smagulova, S. A.; Antonova, I. V. Graphene-Based Humidity Sensors: The Origin of Alternating Resistance Change. *Nanotechnology* **2017**, *28*, No. 355501.
(30) Salehi-khojin, A.; Estrada, D.; Lin, K. Y.; Bae, M.; Xiong, F.; Pop, E.; Masel, R. I. Polycrystalline Graphene Ribbons as Chemiresistors. *Adv. Mater.* **2012**, *24*, 53−57.
(31) Dan, Y.; Lu, Y.; Kybert, N. J.; Luo, Z.; Johnson, A. T. C. Intrinsic Response of Graphene Vapor Sensors. *Nano Lett.* **2009**, *9*, 1472−1475.
(32) Dan, Y.; Lu, Y.; Kybert, N. J.; Luo, Z.; Johnson, A. T. C. Intrinsic Response of Graphene Vapor Sensors. *Nano Lett.* **2009**, *9*, 1472−1475.
(33) Choi, S.; Kim, S.; Kim, I. Ultrafast Optical Reduction of Graphene Oxide Sheets on Colorless Polyimide Film for Wearable Chemical Sensors. *NPG Asia Mater.* **2016**, *8*, No. e315.
(34) Zhang, J.; Liu, X.; Neri, G.; Pinna, N. Nanostructured Materials for Room-Temperature Gas Sensors. *Adv. Mater.* **2016**, *28*, 795−831.
(35) Huang, Y.; Huang, C.; Chen, Y.; Su, C.; Tsai, Y. Effect of Substrate Topography for Graphene-Based Humidity Sensors. *Jpn. J. Appl. Phys.* **2019**, *58*, No. SDDD04.
(36) Phan, D.; Park, I.; Park, A.; Park, C.; Jeon, K. Black P/Graphene Hybrid: A Fast Response Humidity Sensor with Good Reversibility and Stability. *Sci. Rep.* **2017**, *7*, No. 10561.
(37) Hong, G.; Han, Y.; Schutzius, T. M.; Wang, Y.; Pan, Y.; Hu, M.; Jie, J.; Sharma, C. S.; Mu, U.; Poulikakos, D. On the Mechanism of Hydrophilicity of Graphene. *Nano Lett.* **2016**, *16*, 4447−4453.
(38) Gaiduk, A. P.; Pham, T. A.; Govoni, M.; Paesani, F.; Galli, G. Electron Affinity of Liquid Water. *Nat. Commun.* **2018**, *9*, No. 247.
(39) Xu, K.; Cao, P.; Heath, J. R. Graphene Visualizes the First Water Adlayers on Mica at Ambient Conditions. *Science* **2010**, *329*, 1188−1191.
(40) Ma, T. P.; Dressendorfer, P. V. *Ionizing Radiation Effects in MOS Devices and Circuits*; Wiley: New York, 1989.
(41) Aitken, J. M.; Young, D. R.; Pan, K. Electron Trapping in Electron-Beam Irradiated SiO_2. *J. Appl. Phys.* **1978**, *49*, 3386−3391.
(42) Sethi, R. B.; Young, D. R.; Zook, J. D. Charge Trapping In Ion-Sputtered Silicon Dioxide Films On Silicon. *J. Electron. Mater.* **1990**, *19*, 231−234.
(43) DiMaria, D. J.; Cartier, E.; Arnold, D. Impact Ionization, Trap Creation, Degradation, and Breakdown in Silicon Dioxide Films on Silicon. *J. Appl. Phys.* **1993**, *73*, 3367−3384.
(44) Cho, B. J.; Chong, P. F.; Chor, E. F.; Joo, M. S.; Yeo, I. S.; Cho, B. J.; Chong, F.; Chor, E. F. Electron-Beam Irradiation-Induced Gate

Oxide Degradation Electron-Beam Irradiation-Induced Gate Oxide Degradation. *J. Appl. Phys.* **2000**, *88*, No. 6731.
(45) Tarrach, F.; Ch'hayder, A.; Guermazi, S. Charge Trapping and AC Conductivity in Amorphous Silicon Oxide. *Phys. Procedia* **2009**, *2*, 941−945.
(46) Li, H.; Liu, C.; Zhang, Y.; Qi, C.; Wei, Y.; et al. Electron Radiation Effects on the Structural and Electrical Properties of MoS_2 Field Effect Transistors. *Nanotechnology* **2019**, *30*, No. 485201.

https://dx.doi.org/10.1021/acssensors.0c01441
ACS Sens. 2020, 5, 2940−2949